

## THE IONIZED GAS IN THE AFTERMATH OF A STARBURST: THE CASE OF NGC 1569

DANIEL DEVOST, JEAN-RENÉ ROY,<sup>1</sup> AND LAURENT DRISSEN<sup>1</sup>

Département de physique and Observatoire du mont Mégantic, Université Laval, Québec, PQ G1K 7P4, Canada;  
ddevost@phy.ulaval.ca, jrroy@phy.ulaval.ca, ldrissen@phy.ulaval.ca

Received 1996 October 11; accepted 1997 January 23

### ABSTRACT

Results from multislit optical spectroscopy of 16 H II regions and deep H $\alpha$  imaging of the amorphous galaxy NGC 1569 are presented. The extinction across the main body of the galaxy, as derived from the Balmer H $\alpha$ /H $\beta$  line ratio, indicates that most of the observed extinction is taking place in our own Galaxy; the latter amounts to  $(A_V)_{\text{local}} = 1.61 \pm 0.09$ , while the extinction due to NGC 1569 is  $(A_V)_{\text{intrinsic}} = 0.65 \pm 0.04$ . The electron temperature was measured in three H II regions using the [O III]  $\lambda$ 4363 line. The O/H distribution shows no gradient along the main axis of the galaxy, which is consistent with the behavior observed in other low-mass galaxies. The average metal abundance is  $12 + \log \text{O/H} = 8.26$ , with little scatter, suggesting, on one hand, that mixing mechanisms are very efficient throughout the main body of the galaxy, or, on the other, that the most recent nucleosynthetic products are hiding in a hot coronal gas phase. Up to  $20\% \pm 4\%$  of the global H $\alpha$  emission originates from the faint diffuse halo component surrounding the main body of NGC 1569. We explore the possibility that runaway OB stars that are due to cluster ejection and associated with the burst of supernovae which ended  $\sim 5 \times 10^6$  yr ago could be responsible for most of the ionization of the halo gas.

*Subject headings:* galaxies: abundances — galaxies: individual (NGC 1569) — galaxies: ISM — galaxies: starburst — H II regions

### 1. INTRODUCTION

The starburst galaxy NGC 1569, a blue compact dwarf galaxy, has become one of the best studied nearby galaxies (Israel 1988; Israel & de Bruyn 1988; Israel & van Driel 1990; Waller 1991; O’Connell, Gallagher, & Hunter 1994; Drissen, Roy, & Moffat 1993; Heckman et al. 1995; Hunter & Gallagher 1996; Ho & Filippenko 1996). The spectacular appearance of the whole galaxy at optical wavelengths and the presence of a bright radio halo (Israel & de Bruyn 1988), which shows all the features of recent dramatic events—probably an episode of violent star formation—justify in large part this interest. This galaxy is also near enough (2.5 Mpc) for its brightest stars and clusters to be resolved by the *Hubble Space Telescope* (O’Connell et al. 1994). In particular, the presence of many OB associations, in the center of the galaxy of two compact super star clusters (Ables 1971; Arp & Sandage 1985; Ho & Filippenko 1996), “light up” the ISM of NGC 1569 and its surroundings, allowing studies of the physical properties of dwarf starbursting galaxies.

The recent work of Heckman et al. (1995) has brought together a fine ensemble of the known properties of the galaxy by adding new X-ray imaging data from *ROSAT* to produce a clearer picture of the recent evolution of this galaxy. Heckman et al. have proposed a model of a starburst-driven outflow to explain the observed kinematics of the H $\alpha$ -emitting gas and most of the diffuse X-ray halo of the galaxy. Indeed, NGC 1569 is an object the study of which may give insight into both the starburst phenomenon at moderately low metallicity and the magnitude of the impact of the starburst phenomenon on the evolution of dwarf galaxies (Marlowe et al. 1995). This is particularly

relevant in the light of a scenario in which small galaxies are the building blocks of larger ones.

Many massive stars and a gas-rich ISM make the high Balmer luminosity a striking feature of NGC 1569. The spectrum of the nonthermal radio emission, the paucity of O and Wolf-Rayet stars, and the behavior of the H $\alpha$  emission allowed Israel (1988), Israel & de Bruyn (1988), Waller (1991), and Heckman et al. (1995) to reconstruct the evolution of the recent star formation rate (SFR). These authors concur that a major burst occurred 10–20 Myr ago with a  $\text{SFR} \geq 2 M_{\odot} \text{ yr}^{-1}$ . Massive star formation is still active today but is taking place at a slower rate; Waller (1991) estimated the present SFR to be  $0.4 M_{\odot} \text{ yr}^{-1}$ , assuming a coeval star formation episode. Analysis of the synchrotron radiation reveals that a sharp decrease in relativistic electron injection rates took place about  $5 \times 10^6$  yr ago; this has been interpreted as the end of an epoch of intense supernova activity following the starburst (Israel & de Bruyn 1988). The kinematics of the gas does reflect the mechanical energy input of massive stars: de Vaucouleurs (1981), and more recently Tomita et al. (1994), mapped the H $\alpha$  velocity component at high spectral resolution and showed that there are expanding bubbles in the center of the galaxy with typical velocities for the H $\alpha$  gas of  $\simeq 50 \text{ km s}^{-1}$ . This gas is mainly associated with the bright H $\alpha$  emission of NGC 1569. Heckman et al. (1995) confirmed these results and found moderately high-velocity gas ( $\simeq 200\text{--}300 \text{ km s}^{-1}$ ) in the halo, as well as a gas component surrounding the galaxy which is hot enough to give rise to X-ray emission.

The strong nebular features in the spectrum of NGC 1569 provide a reliable indication of the oxygen abundance, temperature, and density of the interstellar medium of the galaxy. Hunter et al. (1982) derived an oxygen abundance of 1/5 solar with the method of Dufour (1975). However, not much is known about the spatial variations of the nebular properties in this galaxy where the interstellar medium has gone through major recent upheavals. To achieve a more

<sup>1</sup> Visiting Astronomer, Canada-France-Hawaii Telescope, which is operated by the National Research Council of Canada, the Centre National de la Recherche Scientifique of France, and the University of Hawaii.

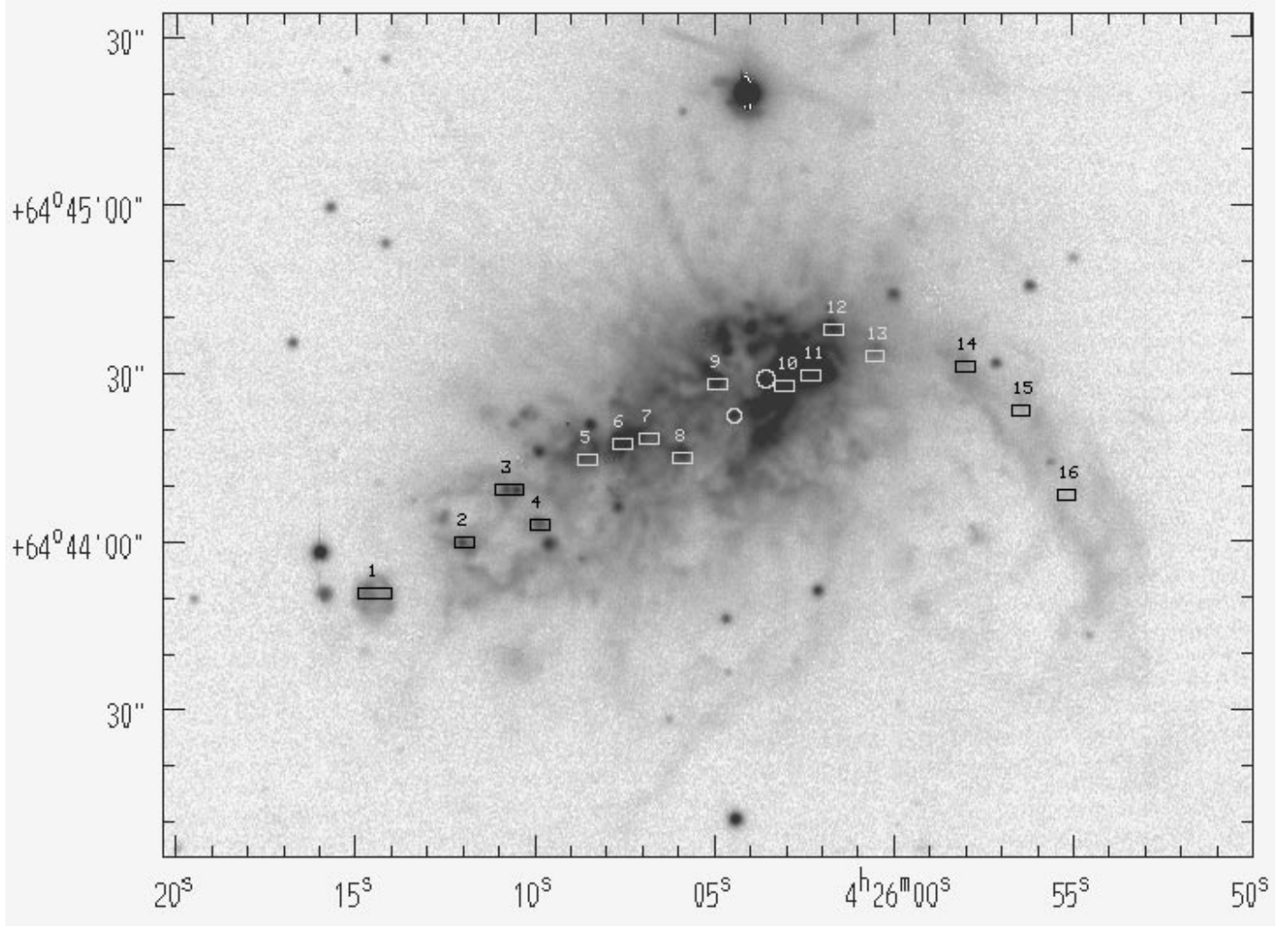


FIG. 1.—MOS aperture locations superposed on a CFHT [O III]  $\lambda 5007$  image of NGC 1569. The circles correspond to star cluster A (*large circle*) and B (*small circle*). The spectral dispersion ran vertically. Coordinates are for 1950.

TABLE 1  
SLITLET POSITIONS IN NGC 1569

Aperture Number	$\Delta x$ (pixels)	$\Delta y$ (pixels)	$\alpha(1950)$	$\delta(1950)$	Name
1 .....	0.0	0.0	4 26 14.	64 43 51.	Waller 12
2 .....	51.5	29.0	4 26 12.0	64 44 00	Waller 11
3 .....	77.0	58.0	4 26 10.8	64 44 10	Waller 9
4 .....	94.4	40.0	4 26 10.0	64 44 04	Waller 8
5 .....	121.5	77.8	4 26 08.8	64 44 16	
6 .....	141.4	87.4	4 26 07.6	64 44 19	Waller 7
7 .....	156.6	90.0	4 26 06.9	64 44 20	
8 .....	175.5	79.0	4 26 05.9	64 44 16	Waller 6
9 .....	195.6	120.7	4 26 05.0	64 44 29	
10 .....	233.7	119.6	4 26 03.2	64 44 29	Waller 3
11 .....	248.5	126.3	4 26 02.4	64 44 31	Waller 2
12 .....	261.8	152.4	4 26 01.8	64 44 39	Waller 1
13 .....	285.0	137.4	4 26 00.6	64 44 35	
14 .....	336.3	130.6	4 25 58.1	64 44 33	
15 .....	367.8	106.3	4 25 56.6	64 44 25	
16 .....	393.8	58.1	4 25 55.4	64 44 10	

NOTE.—Units of right ascension are hours, minutes, and seconds, and units of declination are degrees, arcminutes, and arcseconds.

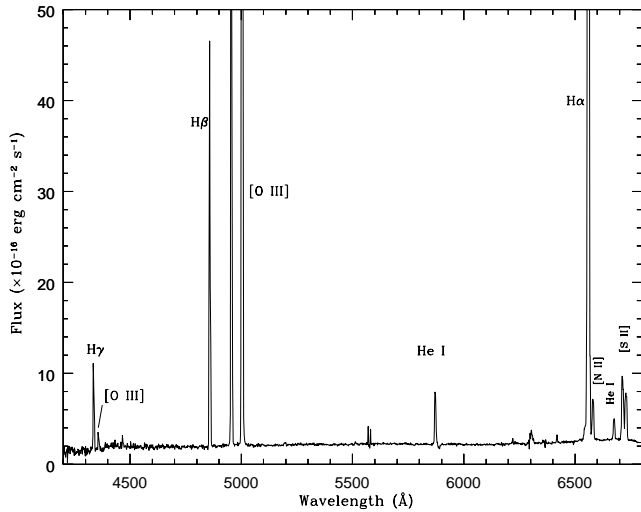


FIG. 2.—Reduced spectrum of the region corresponding to aperture 6

extensive coverage of the properties of the ionized gas and of the massive star content of NGC 1569, we carried out a spectroscopic survey of 16 H II regions along the main axis of the galaxy and of the western ionized gas filament.

## 2. OBSERVATIONS

Images in [O III]  $\lambda 5007$  (FWHM = 15 Å) and continuum light (short exposure with no filter) were obtained of NGC

1569 using the multiobject spectrograph (MOS) at the Canada-France-Hawaii Telescope during the night of 1993 January 19–20 (Fig. 1). Sixteen slitlets were made with a laser-cutting machine in a focal mask to correspond to regions of high nebular surface brightness as seen in the [O III] image. The final positioning of the slits was done employing a short-exposure image in the continuum to ensure, wherever applicable, to include as much of the continuum light of the related stellar associations or clusters in each slitlet. We did not include the bright stellar clusters A and B (Arp & Sandage 1985; O’Connell et al. 1995; Ho & Filippenko 1996) since we felt that the clusters were already too old to hold an important surviving population of very massive stars such as WR stars. A few additional slits were located away from the galaxy to enable subtraction of the background sky spectrum.

We employed the CFHT Lick 2K  $\times$  2K CCD which led to a pixel size along the slit of  $0''.31$ . The B600 grism gave a dispersion of 1.6 Å per pixel, and the resolution allowed by the slit was 8 Å. Unfortunately, the Lick CCD has no response below 4000 Å, and the usable range of the spectrum was from 4300 to 7000 Å; thus, we could not measure the [O II]  $\lambda 3727$  line nor any other nebular lines blueward of H $\gamma$ . Three consecutive exposures of 2000 s were obtained.

The multislit spectra were reduced using standard procedures in IRAF. The CCD images were flat-fielded using exposures of an internal screen illuminated by a quartz lamp. He-Ar arc lamp images were used to calibrate the

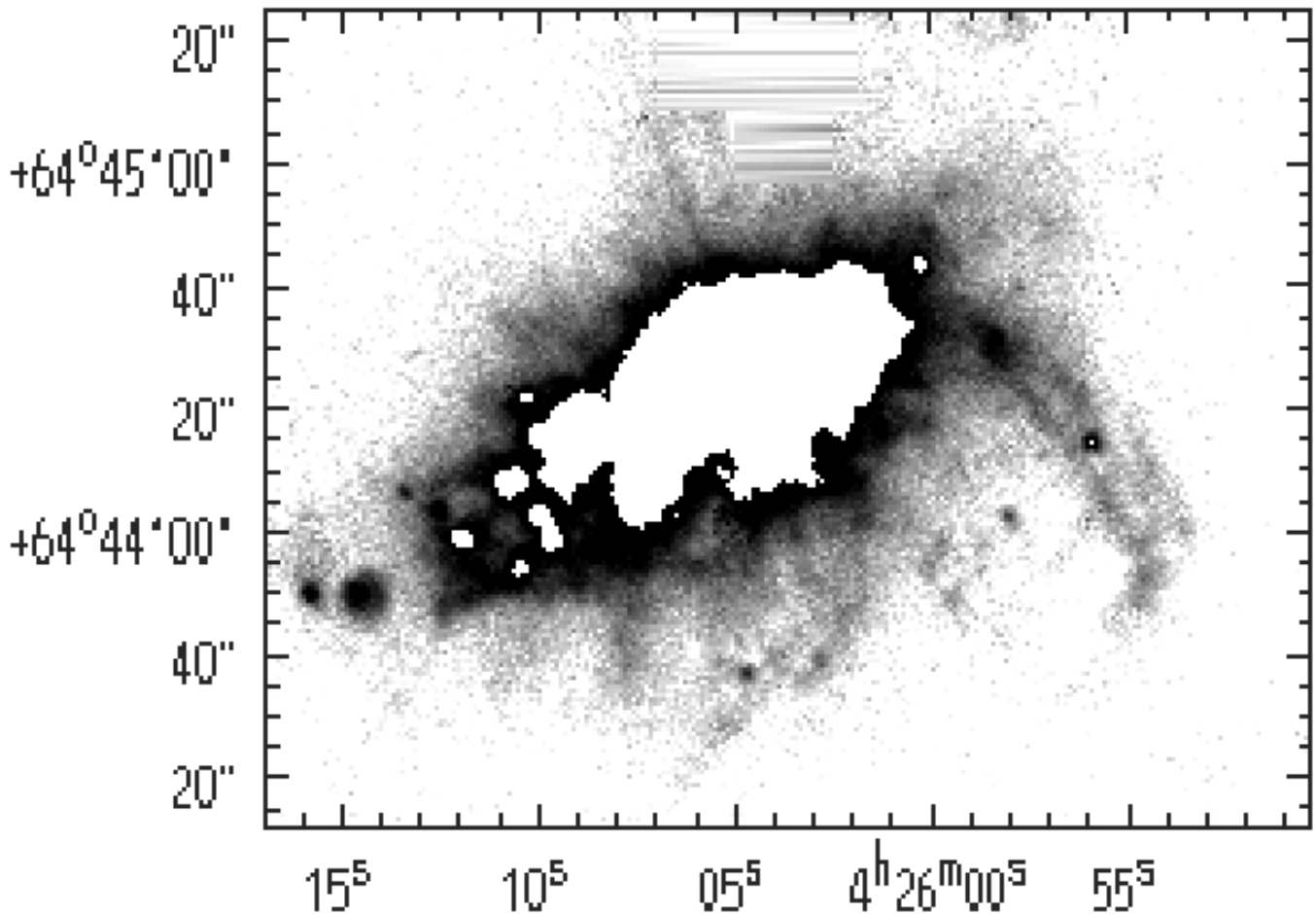


FIG. 3.—H $\alpha$  image of NGC 1569 with the brightest area masked to illustrate the area that we defined as “halo” emission. The horizontal structures result from the mechanical mask employed to hide the star BD64450. Coordinates are for 1950.

TABLE 2  
EXTINCTION CORRECTED FLUXES ( $F(H\beta) = 100$ )

Aperture Number	$-EW(H\beta)$	$c$	4340 Å H $\gamma$	4363 Å [O III]	4861 Å H $\beta$	5007 + 4959 Å [O III]	5875 Å He I	6548 + 6583 Å [N II]	6678 Å He I	6716 Å [S II]	6731 Å [S II]
1	100 ± 2	0.74 ± 0.04	...	...	100 ± 2	466 ± 7	13.6 ± 0.3	16.5 ± 0.4	5.6 ± 0.3	21.1 ± 0.5	14.7 ± 0.4
2	80 ± 2	1.10 ± 0.05	...	...	100 ± 2	630 ± 10	12.5 ± 0.3	11.5 ± 0.4	3.2 ± 0.2	13.4 ± 0.4	11.5 ± 0.3
3	111 ± 2	1.19 ± 0.04	...	...	100 ± 2	690 ± 10	8.8 ± 0.2	11.0 ± 0.3	2.2 ± 0.1	13.2 ± 0.3	8.6 ± 0.2
4	50 ± 2	1.21 ± 0.05	...	...	100 ± 2	513 ± 9	12.4 ± 0.3	16.5 ± 0.4	3.6 ± 0.2	19.6 ± 0.4	14.1 ± 0.3
5	65 ± 2	0.92 ± 0.03	49 ± 1	...	100 ± 2	569 ± 7	10.1 ± 0.2	18.4 ± 0.4	3.2 ± 0.2	27.1 ± 0.4	15.3 ± 0.3
6	117 ± 1	1.16 ± 0.02	35 ± 1	4.9 ± 0.3	100 ± 1	745 ± 5	10.2 ± 1	9.4 ± 1	3.3 ± 0.1	11.6 ± 0.1	8.6 ± 0.1
7	30 ± 2	1.17 ± 0.03	46 ± 1	...	100 ± 2	679 ± 8	10.9 ± 0.3	16.0 ± 0.3	2.5 ± 0.2	17.9 ± 0.3	14.5 ± 0.3
8	35 ± 1	0.91 ± 0.03	42 ± 1	...	100 ± 1	766 ± 8	10.5 ± 0.2	17.7 ± 0.3	3.7 ± 0.2	16.1 ± 0.3	11.4 ± 0.2
9	63 ± 1	1.01 ± 0.02	45 ± 1	...	100 ± 1	714 ± 5	12.5 ± 2	12.9 ± 0.2	3.7 ± 0.1	...	...
10	29 ± 1	0.96 ± 0.02	48 ± 1	11 ± 1	100 ± 1	756 ± 6	9.5 ± 0.2	11.7 ± 0.2	3.2 ± 0.1	...	...
11	171 ± 1	0.99 ± 0.01	38.8 ± 0.5	6.5 ± 0.2	100 ± 1	734 ± 3	9.4 ± 0.1	8.3 ± 0.1	4.0 ± 0.1	...	...
12	44 ± 1	1.13 ± 0.03	46 ± 1	...	100 ± 1	611 ± 7	12.5 ± 0.2	20.0 ± 0.3	...	...	...
13	39 ± 2	1.14 ± 0.05	...	...	100 ± 2	740 ± 10	8.8 ± 0.3	19.2 ± 0.5	...	...	...
14	52 ± 4	0.90 ± 0.07	...	...	100 ± 4	580 ± 20	11.4 ± 0.5	32 ± 1	...	...	...
15	59 ± 5	0.8 ± 0.1	...	...	100 ± 5	500 ± 20	11.1 ± 0.6	25 ± 1	...	...	...
16	50 ± 8	0.9 ± 0.2	...	...	100 ± 8	650 ± 40	...	19 ± 2	...	35 ± 2	20 ± 2

spectra in wavelength and to rectify geometrically the images. Because the slitlets fall at positions spread across the field, the wavelength calibration procedure cannot correct optical distortions in the direction perpendicular to the dispersion axis. To make this correction, the light distribution across each slitlet was fitted with a Gaussian profile; the center of the Gaussian was then used to straighten the spectra along dispersion. This method, which is not ideal, worked reasonably well, as is verified by our ability to subtract the bright emission lines from the sky background. A spectrum of the spectrophotometric star Feige 34 was used to flux calibrate the spectra.

The locations of the slits over the main body of the galaxy are shown in Figure 1. The size of slits number 2 and 4 to 16 is  $1''.6 \times 3''.3$ , which corresponds to  $20 \text{ pc} \times 40 \text{ pc}$  on the galaxy, at the assumed distance of 2.5 Mpc (O'Connell et al. 1994); slit number 1 has a size of  $1''.6 \times 6''.0$ , corresponding to  $20 \times 72 \text{ pc}$  on the galaxy, and slit number 3 has  $1''.6 \times 4''.9$  or  $20 \times 59 \text{ pc}$ . The astrometric positions (based on the astrometry of Waller 1991) of the centers of the slits are given in Table 1. The seeing was  $1''.2$  the night of the spectroscopic observations.

The reduced spectrum of aperture 6 is shown in Figure 2; the H $\alpha$ , H $\beta$ , and [O III]  $\lambda\lambda 4959, 5007$  lines are detected with a high S/N ratio. A similar level of S/N ratio is typical of the 16 spectra for these lines. We lost the [S II]  $\lambda\lambda 6716, 6731$  lines on six spectra (apertures 9–14) as the result of field limitation.

H $\alpha$  ( $\lambda_0 \approx 6561 \text{ \AA}$ , FWHM =  $10 \text{ \AA}$ ) images were obtained with the 1.6 m telescope at the Observatoire du Mont Mégantic (OMM) during the nights of 1994 August 29–30 and October 1–2 using a  $f/8 \rightarrow f/3.5$  focal reducer and a Thomson CCD (1 K × 1 K); the scale was  $0''.7$  per pixel. The image resulting from three exposures of 2000 s is shown in Figure 3; the continuum was subtracted using an emission-line-free image at  $7020 \text{ \AA}$  (FWHM =  $200 \text{ \AA}$ ). Reduction of the images was done using the usual procedures in IRAF.

### 3. RESULTS

#### 3.1. Spectroscopic Data

Emission-line fluxes were measured by integrating the counts over each line profile and by subtracting a linear fit

to the underlying continuum employing the SPLOT routine in IRAF. We derived reddening using the H $\alpha$  and H $\beta$  Balmer decrement assuming case B of the recombination theory, a temperature of 10,000 K, and an electron density of  $100 \text{ cm}^{-3}$ . The logarithmic extinction values ( $c$ ) were then used to correct all the other line fluxes relative to  $F(H\beta)$  using Kinney's law (Kinney 1994). No correction was applied for underlying Balmer absorption since the equivalent width of H $\beta$  is generally high in the regions of NGC 1569 that we sampled (see Table 2). The corrected fluxes of the brightest lines, normalized to the flux at H $\beta$  and the logarithmic extinction at H $\beta$ ,  $c$ , are listed for each slitlet on the galaxy (numbered 1–16) in Table 2. The corrected H $\gamma$  fluxes and errors are also given to get a feeling of the accuracy of the reddening corrections.

The [O III]  $\lambda 4363$  was detected in six of the spectra (slits 3, 6, 8, 9, 10, and 11) and could be measured with sufficient S/N in regions 6, 10, and 11 (Table 3). Line ratios measured with a S/N ratio less than 5 were not used in deriving physical parameters (see Rola & Pelat 1994). With the five-level atom approximation, we calculated the density and electron temperature using, respectively, the [S II]  $\lambda 6716$ /[S II]  $\lambda 6731$  and the [O III]  $\lambda\lambda 4959, 5007$ /[O III]  $\lambda 4363$  line ratios. The abundance indicator [O III]/[N II] as calibrated by

TABLE 3  
PHYSICAL PARAMETERS

Aperture Number	$\rho_e(\text{cm}^{-3})$	$T_e$ (K)	$12 + \log(\text{O}/\text{H})$
1	<100	...	8.32 ± 0.07
2	302 $^{+82}_{-73}$	...	8.2 ± 0.2
3	<100	...	8.2 ± 0.1
4	<100	...	8.3 ± 0.1
5	<100	...	8.31 ± 0.06
6	<100	11100 $^{+215}_{-240}$	8.14 ± 0.08
7	218 $^{+41}_{-25}$	...	8.26 ± 0.08
8	<100	...	8.26 ± 0.07
9	...	...	8.22 ± 0.07
10	...	15000 $^{+991}_{-763}$	8.19 ± 0.08
11	...	12300 $^{+163}_{-117}$	8.12 ± 0.03
12	...	...	8.31 ± 0.05
13	...	...	8.3 ± 0.1
14	...	...	8.37 ± 0.08
15	...	...	8.4 ± 0.1
16	<100	...	8.3 ± 0.2

Edmunds & Pagel (1984) was used to derive the O/H abundances in all regions since we do not have [O II]  $\lambda 3727$  measurements. The values calculated are listed in Table 3. Column (2) gives the electronic density derived from the sulphur line ratio with the de Robertis et al. (1987) five-level atom program that uses the Cai & Pradhan (1993) atomic data; the electron density of the ISM of NGC 1569 is generally consistent with the low-density limit, but it reaches a few hundred  $\text{cm}^{-3}$  at positions of slits 2 and 7. Column (3) gives the electron temperature of the three H II regions where the S/N ratio was sufficiently high. The code of de Robertis et al. (1987) was used again, but this time with the atomic data of Mendoza (1983).

Column (4) shows the oxygen abundance at each slit. The quoted errors on O/H are those propagated from the errors on the [O III]/[N II] line ratios. The real uncertainties on the abundances of O/H is probably larger and is determined by the uncertainty in the calibration of the [O III]/[N II] indicator. The [O III]/[N II] line ratio has been shown to be a reliable indicator of O/H, particularly at the level of abundances corresponding to  $12 + \log \text{O/H} \sim 8.0\text{--}8.4$  (Roy et al. 1996). However, this indicator is sensitive to the intrinsic scatter of the ionization parameter and to the scatter in the N/O versus O/H abundance relation at low abundances (Dopita & Evans 1986; Garnett 1990). The small scatter of [O III]/[N II] across NGC 1569 may be due either to the small dispersions of O/H abundances, ionization parameters, and/or N/O across the galaxy, or to a conspiracy where the variations of each factor tend to cancel each other. Looking at Table 3, one sees that  $12 + \log (\text{O/H})$ , as determined from [O III]/[N II], is lowest for the three apertures with measured electron temperatures. Thus, if [O III]/[N II] is giving us reliable information about O/H, abundances may indeed vary slightly; smaller oxygen abundances reduce cooling, which results in higher electron temperatures, thus stronger [O III]  $\lambda 4363$ . On the other hand, there could be a systematic effect in the empirical calibration or a systematic overestimate of the [O III]  $\lambda 4363$  line strength. In irregular galaxies, N/O varies as much as a factor of 3 from galaxy to galaxy (Garnett 1990), but, except for the exceptional case of NGC 5253 (Kobulnicky et al. 1997), no significant fluctuations of N/O within small galaxies have been observed so far.

With these caveats in mind, we conclude that there is no global gradient, and that  $12 + \log (\text{O/H})$  appears relatively uniform over the galaxy, with a mean value of 8.26; this is in agreement with the value previously found by Hunter & Gallagher (1982). The recent observations of NGC 4214 by Kobulnicky & Skillman (1996) reinforces the impression of chemical homogeneity in these types of galaxies.

We also found evidence for a broad pedestal to the [O III]  $\lambda\lambda 4959, 5007$  lines at the position of aperture 6 (Fig. 4). This type of extended broad component is generally attributed to some sort of hypersonic nebular wind, but its exact origin is not known (Roy et al. 1992; Izotov et al. 1996). Heckman et al. (1995) found a broad component at another position associated with cluster A.

### 3.2. Imaging Data

Deep imaging of the galaxy at H $\alpha$  was done to probe the extent of the faint filaments and diffuse emission associated with the galaxy. The image was calibrated by comparing the H $\alpha$  flux in aperture 1 of the CFHT MOS spectra with the counts corresponding to the same area on the OMM image.

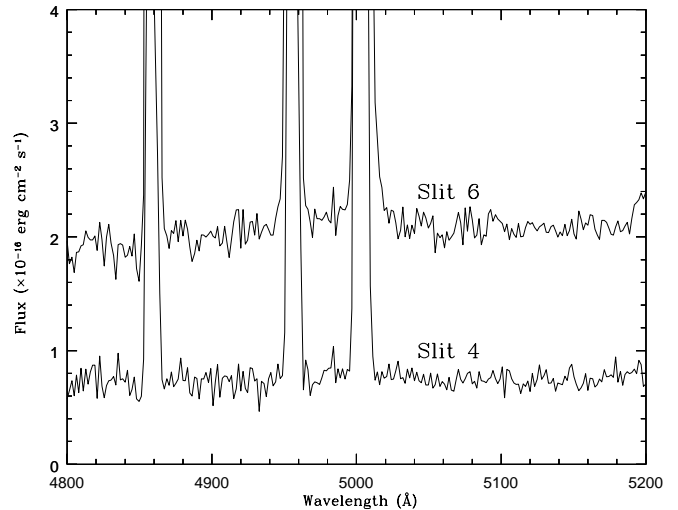


FIG. 4.—The broad pedestal component of the [O III] line of slit 6 (upper spectra) is compared with the nonbroad component of slit 4. Slit 6 is the only spectra where this broad component was found.

Differences in seeing and in sampling introduce uncertainties. We find a value of  $L(\text{H}\alpha) = 10^{41}$  ergs  $\text{s}^{-1}$  for the whole galaxy. The value of  $L(\text{H}\alpha)$  was corrected for total foreground extinction assuming  $A_{\text{H}\alpha} = 1.74$ . Waller (1991) measured  $L(\text{H}\alpha) \sim 4 \times 10^{40}$  ergs  $\text{s}^{-1}$ . The difficulties and unreliability of calibrating the Mont Mégantic image by scaling the flux measured in small slits (CFHT and better seeing) may explain a good part of the discrepancy of a factor of  $\sim 2$ , and we have more confidence in Waller's value.

We calculated the amount of faint H $\alpha$  emission of the halo by masking, from the whole image, the brightest surface emission component ( $\mu > 1.12 \times 10^{-14}$  ergs  $\text{cm}^{-2} \text{s}^{-1} \text{arcsec}^{-2}$ ) (Fig. 3), a level we assumed to be mostly associated with the disk. The definition of the boundary between the faint and bright H $\alpha$  emission is the major contributor to the uncertainty. Up to  $20\% \pm 4\%$  of the total H $\alpha$  emission is diffuse emission from the halo, probably associated with gas ejected from the galaxy during the recent and continuing starburst. This is a lower estimate because we ignore the contribution in the direction of the masked region; the actual fraction of halo emission may reach 30%. Our measurement for the halo emission closely agrees with that of Heckman et al. (1995); these authors have suggested that most of the extraplanar optical emission-line gas is associated with structures in the shape of large expanding shells. Hunter & Gallagher (1996) have reported a similar ratio of escaping ionizing photons in Sextans A, NGC 2366, NGC 4449, and also in NGC 1569.

## 4. DISCUSSION

### 4.1. Dust Content of NGC 1569

Since NGC 1569 is at galactic latitude  $b = 11^\circ 2'$  (Clements 1983), it suffers from a large amount of Galactic extinction. From the UV color-color diagram, Israel (1988) inferred a value of  $E(B-V) = 0.56 \pm 0.10$  for the total extinction. By comparing with the spectrum of BD +64°450, a magnitude 10 star located a few arcminutes north of NGC 1569, he concluded that most of the extinction suffered by NGC 1569 originates from our own Galaxy. Burstein & Heiles (1984), using H I column density,

derived a galactic component equivalent to  $E(B-V) = 0.51$  in the direction of NGC 1569.

The value of  $E(B-V)$  found by Israel corresponds to  $A_V = 1.79 \pm 0.30$ , if one assumes  $R = 3.2$ . Figure 5 displays the value of the total logarithmic and V-band extinction derived from the  $H\alpha/H\beta$  ratio for each of our MOS apertures across the galaxy; the short-dashed line corresponds to the value derived by Israel, with the error bar indicated by long-dashed lines. We calculated the value of  $A_V$  from the  $c$  values obtained in column (2) of Table 2 employing the conversion factor between  $A_V$  and  $c$  of Schild (1977).

Most of the extinction values of NGC 1569 are higher than the upper limit calculated by Israel. All extinction values are higher than that observed at slit 1 (Waller 12), which is well within Israel's error bar and close to the value of  $A_V = 1.79$ . Region Waller 12, which has been shown by Drissen & Roy (1994) to be an unusually large Wolf-Rayet wind-blown bubble, lies on the eastern edge of NGC 1569. We suggest that either the Wolf-Rayet and other massive stars of Waller 12 have punched a hole in the ISM of NGC 1569 or that Waller 12 is located on the front side of the galaxy, both situations leaving the line of sight to Waller 12 obscured mostly by dust that belongs to our own Galaxy. Following this assumption and using the extinction difference of all the other slits with slit 1, we estimate that NGC 1569 has an intrinsic mean extinction value  $\langle A_V \rangle_{\text{intrinsic}} = 0.65 \pm 0.04$  [ $E(B-V) = 0.20$ ] and that the extinction due to our own Galaxy is  $(A_V)_{\text{local}} = 1.61 \pm 0.09$  [ $E(B-V) = 0.50$ ]. These values refer only to foreground screen extinction in the ionized gas.

#### 4.2. $EW(H\alpha)$ and Star Formation History

The variation of  $EW(H\alpha)$ , which is due to the short lifetime of the ionizing stars (see Fig. 43 of Leitherer & Heckman 1995), is a strong function of time, and one can think of it as an age indicator for very young clusters. However, to be valid, a measure of the  $EW(H\alpha)$  must obey some constraints. First, one has to include the whole spatial extent of the studied H II region in order to account for the total nebular  $H\alpha$  emission. For H II regions that extend over

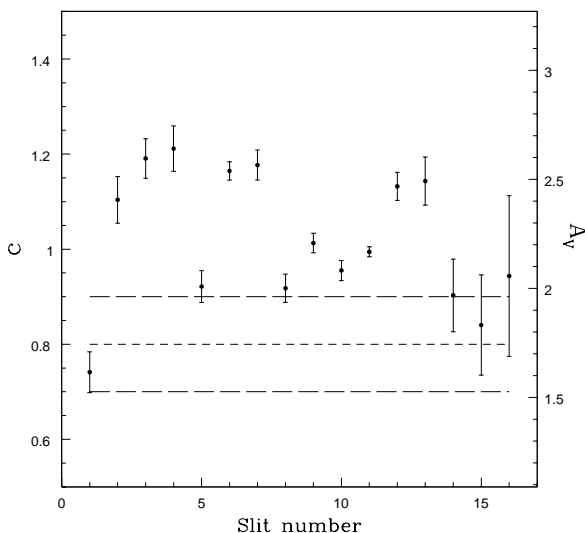


FIG. 5.— $H\alpha/H\beta$  derived extinctions expressed in  $c$  and  $A_V$ . Short-dashed line represents the value calculated by Israel (1988), while long-dashed line represents its uncertainty.

several hundred parsecs, geometrical dilution makes age determination with the  $EW(H\alpha)$  very uncertain. Also, the considered H II region must not be contaminated by the extended  $H\alpha$  emission coming from a neighboring H II region. Such a contamination will lead to false values of age.

Figure 6 is a plot of the contour map of the  $H\alpha$  equivalent width superposed on the *HST*-WF/PC V-band image. The clusters A and B lie in a striking trough of low  $EW(H\alpha)$  surrounded by a horseshoe-shaped crest of high  $EW(H\alpha)$ . Indeed, most of the H II regions surrounding objects A and B have a relatively high value of  $EW(H\alpha)$  and are compact in size; in this case,  $EW(H\alpha)$  should be a good tracer of their age. A scenario of star formation induced by the events which produced clusters A and B can be proposed. O'Connell et al. (1994) found from the colors of the cluster an age  $\leq 15$  Myr for A. Prada et al. (1994), using the Ca II infrared triplet absorption lines and the slope of the continuum, inferred an age of 12 Myr for cluster B and 13–20 Myr for cluster A. We may suppose then that their stellar winds and supernovae formed a shock wave that compressed the surrounding gas and triggered a new star formation episode (Elmegreen 1994). This gave rise to the high  $EW(H\alpha)$  regions that we are observing today that corresponds to an age of 2–4 Myr. On the basis of these assumptions, we then can estimate the delay time, i.e., the time required to produce the supershell and for this shell to become gravitationally unstable; it may be as short as about  $\sim 10$  Myr.

#### 4.3. Dispersal and Mixing

Despite the very disturbed appearance of the interstellar medium related to the recent starburst episode, the O/H abundances are surprisingly uniform over NGC 1569 (see Table 3). The O/H abundances appear identical for all slit positions, i.e., within the 0.2 dex intrinsic uncertainty of the abundance indicator (Edmunds & Pagel 1984). The observed O/H abundances display no gradient along the main axis, and the scatter is small, indicating that dispersal and mixing have been very efficient. Although massive stars are the main source of oxygen and of several other heavy elements, mechanical phenomena associated with their evolution strongly favor their dispersal and mixing in the environment (Roy & Kunth 1995; Tenorio-Tagle 1996). One may speculate that the ISM in NGC 1569 appears presently well homogenized (i) either because the new elements were rapidly dispersed and mixed in the ionized interstellar medium, or (ii), on the contrary, because the new heavy elements, first injected in a hot phase (thus optically undetectable), remain isolated and mix over a long time-scale. In this latter scheme, discussed by Tenorio-Tagle (1996), the most recent products of massive star nucleosynthesis remain unobservable optically. Furthermore, they could move rapidly to the halo or escape from the galaxy through a blowout phase of expanding hot superbubbles (Mac Low & McCray 1988; Koo & McKee 1992).

Let us have a brief look at dispersal. On the 100–1000 pc scale, transport and dispersal are achieved mainly by the sequence of expanding supershells successively enriched by triggered star formation episodes. Diffusion and stirring by Rayleigh-Taylor and Kelvin-Helmholtz instabilities first mix locally the heavy elements released by the OB association with the shell material (Roy & Kunth 1995). Diffusion is very effective in the hot coronal phase of the supernova and wind-blown cavity (Tenorio-Tagle 1996); some 10% of the shell mass is incorporated in this way into the hot cavity.

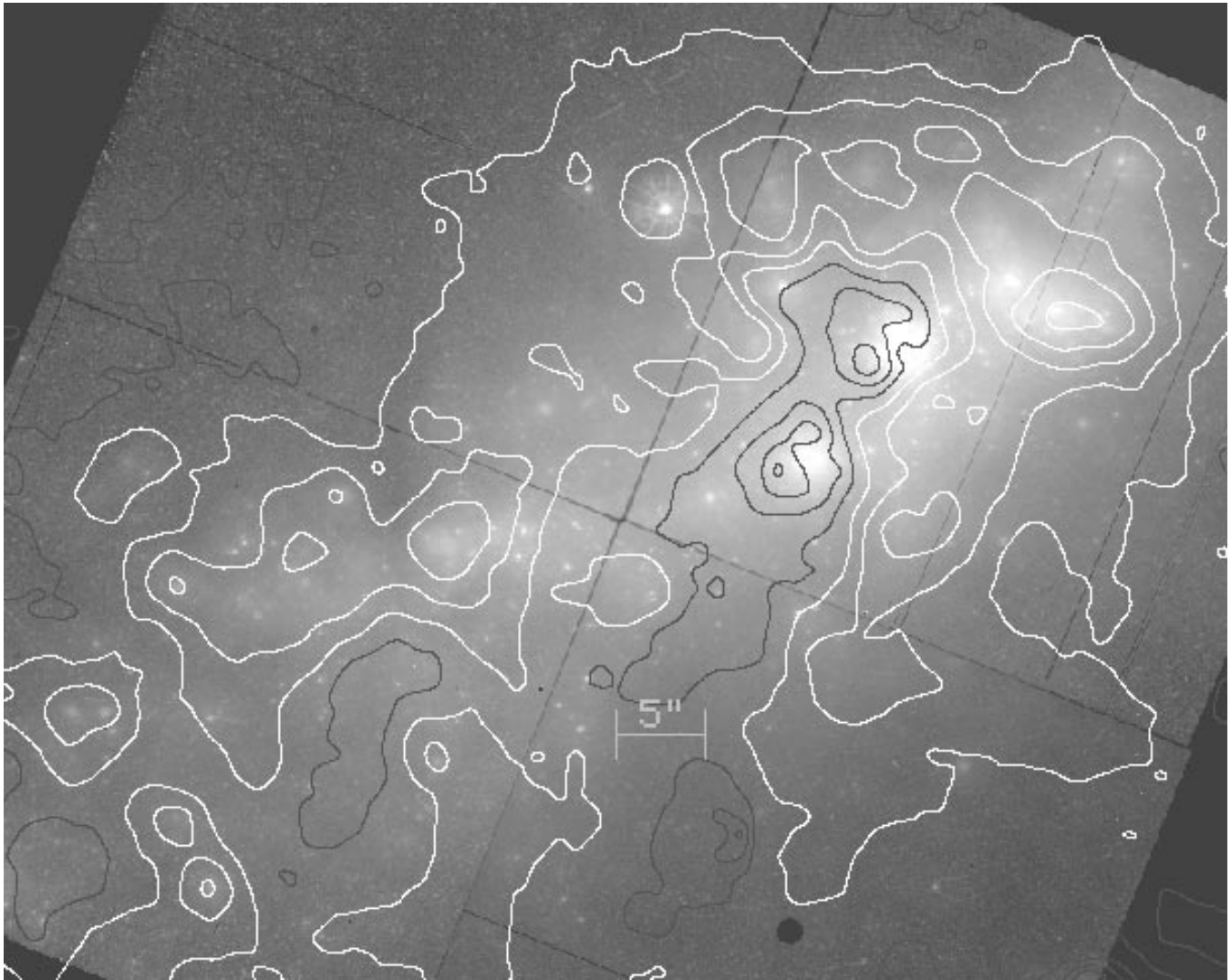


FIG. 6.—Superposition of the EW(H $\alpha$ ) contours on a *HST*-WF/PC V-band image. The black contours show decreasing levels of EW; objects A and B lie in a trough of low EW(H $\alpha$ ). North is up, and east is at left.

Over a long period, cooling by radiation will change the metals into molecular droplets becoming subject to transport by cloud motions.

Moving shells created by stellar winds and supernovae shells act like conveyor belts. Some of these shells become unstable, form new associations, and again move the increasingly enriched gas. Repeated, this sequence corresponds to a pseudo random walk through the galaxy and allows spatial homogenization. Roy & Kunth (1995) have treated this problem assuming no “breakout” or “blowout” out of the disk. For example, a parcel of gas moving continuously in time would random walk over a distance of 750 pc (approximate mean distance from objects A and B to the edge of the galaxy) in  $\sim 300$  Myr; allowing for some dormancy time between star formation events stretches this timescale. Thus, if expanding shells were the only transport mechanism, we should see some abundance fluctuations in NGC 1569 because of the extreme youth of several powerful localized starbursts. Furthermore, allowing “breakout” or “blowout” in some events should enhance the observed scatter in abundances because blowout would strongly depend on the mass and location of the OB associ-

ations or clusters and on the local scale height of the ISM (Koo & McKee 1992).

The main contributor to mixing at larger scale (1–10 kpc) is the azimuthal homogenization of cold clouds done by turbulent transport in the differential rotation of the disk. Using the approach of Roy & Kunth (1995) and assuming that the radial gradient velocity derived by Israel & van Driel (1990) ( $36 \text{ km s}^{-1} \text{ kpc}^{-1}$ ) correspond to a differential shear, the timescale for azimuthal homogenization would be  $\sim 50$  Myr. This again is a *lower* limit because some, if not most, of the steep apparent velocity gradient may be due to solid body rotation in the central parts of the galaxy—which excludes shear. In summary, this time scale and the previous one are much longer than the age of the starburst in NGC 1569; thus, we should see some zones of abundance enhancement since most of the oxygen and other heavy elements are injected in the local ISM within  $10^7$  yr of the birth of a massive star cluster (Lequeux et al. 1981).

We surmise that the new elements produced in the recent starburst in NGC 1569 have been lost, or more likely, that they are hiding in a hot phase. Indeed, observations with *ROSAT* and *ASCA* (Della Ceca et al. 1996) show that

roughly 60% of the soft X-ray emission in NGC 1569 comes from a diffuse, hot gas. The extent of this diffuse X-ray emission mimics the morphology of the H $\alpha$  halo of the galaxy; Della Ceca et al. relate its origin to the galactic superwind emanating from the disk. The recent mechanical energy input has stirred the ISM and mixed heavy elements produced by *previous* generations of star-forming events. However, the “hiding-in-hot-gas” scenario cannot apply to all enrichment events because we would then observe several very low-metallicity objects, which is not the case.

#### 4.4. *The Extended Nebular Emission*

Nebular emission in NGC 1569 extends over several hundred parsecs on either side of the main body of the galaxy, especially perpendicular to the main axis of the stellar body. The observed values of the diagnostic line ratios [N II]/H $\alpha$  and [S II]/H $\alpha$  show that the main source of ionization is from young massive stars (see also Heckman et al. 1995). Hunter & Gallagher (1996) also confirm that photoionization by massive stars dominate the photoionization of the faint extraplanar filament system in irregulars. However, the location and nature of the stars responsible for these ionizing photons is not clear.

Using a Salpeter initial mass function, Israel (1988) estimated that at least  $2 \pm 1 \times 10^6 M_{\odot}$  of O7–K5 stars, formed in the burst, are still visible today. The total H $\alpha$  luminosity of NGC 1569 requires about  $10^{52} \text{ s}^{-1}$  ionizing photons, or the equivalent of 512 O6 V or 6500 O9 V stars (Leitherer 1990). To ionize the diffuse halo gas,  $\geq 20\%$  of the ionizing photons must escape from the disk. The H I map of Israel & van Driel (1990) shows a large amount of neutral gas in the disk; about 45% of the total mass of NGC 1569 appears to be gaseous, and H I column densities are high throughout the galaxy (Israel & van Driel 1990). Despite the clumpiness of the ISM and “holes” in the position-velocity map, it is difficult to have  $\geq 20\%$  of the ionizing photons produced by clusters of OB stars escape freely from the disk. Hunter & Gallagher (1996) have commented on the difficulty of explaining long optical paths for ionizing photons in gas-rich star-forming irregulars.

Simulations with the code of Leitherer & Heckman (1995) clearly demonstrate that to deliver  $10^{52}$  photons  $\text{s}^{-1}$ , a source must be young. Assuming the total mass of stars of clusters A and B to be  $\sim 5 \times 10^5 M_{\odot}$  (Ho & Filippenko 1996), a Salpeter IMF with  $1 M_{\odot} \leq M \leq 100 M_{\odot}$  and  $Z = 1/4 Z_{\odot}$ , we found that after 10 Myr, such objects can only deliver  $3 \times 10^{50}$  ionizing photons; this represents approximately 3% of the photon flux needed to reproduce the observed H $\alpha$  extended nebular flux. Objects A and B cannot ionize the extended gas of NGC 1569.

Instead one may account for the ionization in the faint outer nebular component, if one allows young hot stars to travel above one or more scale heights of gas; lower local and overall densities then permit ionizing photons to travel longer paths, and to ionize much larger volumes because of the reduced recombination rate. Runaway OB stars can raise high enough above the disk and be responsible for the ionization of the nebular halo of NGC 1569. Such stars can be produced by the SN explosion of the most evolved component of a massive close binary, catapulting the remnant out of the original association (Blaauw 1964, 1993), or by single-binary, binary-binary, or *n*-body encounters during the formation of stellar superclusters (Gies & Bolton 1986; van Rensbergen et al. 1996). In this context, it is interesting

to note that a significant fraction of OB stars are found outside of bright H II regions in galaxies such as the Magellanic Clouds (Massey et al. 1995) or M33 (Patel & Wilson 1995); the origin of these stars is unclear, but they could have been formed in situ or could have been ejected from their parent cloud by mechanisms mentioned above.

Because of its low mass, the escape velocity of NGC 1569 is small, i.e., in the range 50–100 km  $\text{s}^{-1}$ , as discussed in Heckman et al. (1995). Thus, typical velocities of runaway stars, which are  $\geq 40$  km  $\text{s}^{-1}$  and can reach up to 200 km  $\text{s}^{-1}$  (Stone 1979; Blaauw 1993), will allow these stars to make large excursions away from their birth place. To explain the ionized halo of NGC 1569, we suggest a burst of runaway OB stars associated with the high supernova rate that ended about 5 Myr ago (Israel & de Bruyn 1988). Assuming that the fraction of O stars which became runaway is the same as in our Galaxy, i.e.,  $\sim 20\%$  for O types down to 2.5% for B0–B0.5 (Gies & Bolton 1986; Blaauw 1993) leads to several hundred OB stars potentially able to reach the halo. For NGC 1569 two extreme cases can be considered: the star can travel along the semimajor ( $d \simeq 1$  kpc) or the semiminor ( $d \simeq 200$  pc) axes. Runaway stars ejected from their parent clusters at speeds of 50 km  $\text{s}^{-1}$  would cross the semimajor axis in  $\sim 20$  Myr and the semiminor axis in  $\sim 5$  Myr. Consequently, O6 stars and later type stars moving more or less perpendicular to the major axis will have enough time to rise above the gas-rich disk. Of the equivalent 6500 O9 V stars accounting for the present total H $\alpha$  luminosity of NGC 1569, we estimate that  $\sim 1/10$  of these are runaway stars which have risen high enough above the gas disk (we suppose that trajectories must have at least an angle of  $45^\circ$  with respect to the galaxy plane to get high enough for contribution to the ionization of the halo gas). How large a volume could be ionized by such a population of extraplanar runaway equivalent 6500 O9 V stars? The Strömgren sphere of individual late O and early B spectral types is  $\sim 30$  pc in a gas of  $1 \text{ cm}^{-3}$  uniform density; consequently, the inferred number of runaway OB stars could ionize the equivalent of a Strömgren sphere  $\sim 400$  pc in diameter. With a mean lifetime of 10 Myr, O9 stars can reach 400 pc, well into the halo where density is probably much less than  $1 \text{ cm}^{-3}$  high above the disk, and the ionized region could extend further. Earlier type stars (O6) do not live long enough to get that high, but they produce more ionizing photons. This scenario is applicable to other star-forming low-mass and irregular galaxies showing intricate sets of ionized shells and filaments.

#### 4.5. *Wolf-Rayet Stars*

The presence of Wolf-Rayet stars in the integrated light of young star clusters is usually detected by the strong, large emission-line complex at  $\sim 4680 \text{ \AA}$  (the “WR bump”; Smith 1991), which includes the He II  $\lambda 4686$  line, blended with nitrogen or carbon lines. Other lines in the yellow and red, such as C III  $\lambda 5800$ , He I  $\lambda 5876$ , He I  $\lambda 6678$ , or even a broad H $\alpha$  line can also betray the presence of WR stars, but these lines are usually weaker than the 4680  $\text{Å}$  bump.

Although one of our objectives was to identify the Wolf-Rayet star clusters potentially associated with the several star-forming regions in NGC 1569, the low sensitivity of the CCD blueward of  $\sim 4800 \text{ \AA}$ , combined with the large reddening toward NGC 1569, prevented us from detecting the blue part of the stellar continuum except in slits 7, 10, 1, and 12. Broad He I emission lines (at 5876 and 6678  $\text{Å}$ ) were

detected at the center of slit 1 (Drissen & Roy 1994); a new analysis of the same data also shows a broad C III feature at 5800 Å, confirming the presence of at least one WR star at that location. A weak emission feature is detected in slit 7 at 4681 Å; it is slightly larger than nebular emission lines (FWHM = 12 Å compared with 8 Å), but it seems too narrow to be due to a Wolf-Rayet star. A close look at the *HST* images of NGC 1569 (O'Connell et al.) shows that the continuum source in slit 7 is a small cluster including a very blue star. It is also coincident, within the errors, with an X-ray source (Heckman et al. 1995).

The other slits do not show any evidence for Wolf-Rayet features; therefore, the bubble sampled by slit 1 remains the only region in NGC 1569 where Wolf-Rayet-like stars have been detected (Drissen & Roy 1994). However, we feel that neither the spectroscopic observations presented here nor the narrow-band imagery of Drissen, Roy, & Moffat (1993) do allow us to completely dismiss the existence of Wolf-Rayet stars in NGC 1569. A detailed mapping of the Wolf-Rayet population in NGC 1569 would help in assessing the star formation history during the most recent starburst episode.

### 5. CONCLUSIONS

NGC 1569 is a relatively metal poor object with a moderately low dust content. It experienced two recent episodes of star formation: the earliest of the two led to the formation of objects A and B 10–20 Myr ago and a peak supernova rate terminating about 5 Myr ago. The main star-forming event produced at least  $2 M_{\odot} \text{ yr}^{-1}$  of stars. The highest EW(H $\alpha$ ) objects observed now have a mean SFR of  $0.4 M_{\odot} \text{ yr}^{-1}$  and correspond to the present episode of star forma-

tion, the latest one. The stellar winds and supernovae of the earlier episode may have triggered the present episode by the phenomenon of compression-induced gravitational instability.

The O/H abundance apparent uniformity ( $\approx 1/5$  solar) across the galaxy suggests that the most recent nucleosynthetic products are not mixed with the local medium on a short timescale ( $\leq 10^{6-7}$  yr) but may instead hide in the hot coronal phase produced by the shocks associated with stellar winds and supernovae-driven bubbles. This apparent uniformity of metal abundances in NGC 1569 supports the scenario of Tenorio-Tagle (1996) of long mixing time involving successive generations of massive stars: a given generation introduces the new elements in a hot phase, which upon cooling by radiation leads to condensation into small molecular droplets. These are then dispersed over the long term by motions of clouds and by differential rotation (as discussed by Bateman & Larson 1993; Roy & Kunth 1995; Tenorio-Tagle 1996); final mixing occurs when a new generation of stars destroys the droplets and diffuses them into a new H II region. Finally, we showed that runaway OB stars rising above very few scale heights of interstellar gas could be responsible for the ionization of the ionized diffuse and filamentary extraplanar gas.

Discussions with Carmelle Robert and Lex Kaper were most fruitful. We thank the referee for helpful comments and suggestions. This investigation was funded by the Natural Sciences and Engineering Research Council of Canada and the Fonds FCAR of the Government of Québec. D. D. is thankful to the STScI and in particular to Claus Leitherer, for hospitality during his stay when part of this work was accomplished.

### REFERENCES

- Ables, H. 1971, *Publ. US Naval Obs.*, 20, 61  
 Arp, H. C., & Sandage, A. 1985, *AJ*, 90, 1163  
 Bateman, N. P. T., & Larson, R. B. 1993, *ApJ*, 407, 634  
 Blaauw, A. 1964, *ARA&A*, 2, 213  
 ———. 1993, in *ASP Conf. Proc. 35, Massive Stars: Their Lives in the Interstellar Medium*, ed. J. Cassinelli & E. Churchwell (San Francisco: ASP), 207  
 Burstein, D., & Heiles, C. 1984, *ApJS*, 54, 33  
 Cai, W., & Pradhan, A. K. 1993, *ApJS*, 88, 329  
 Clements, E. D. 1983, *MNRAS*, 204, 811  
 Della Ceca, R., Griffiths, R. E., Heckman, T. M., & MacKenty, J. W. 1996, *ApJ*, 469, 662  
 de Robertis, M. M., Dufour, R., & Hunt, R. 1987, *JRASC*, 81, 195  
 de Vaucouleurs, G. 1981, *S&T*, 62, 406  
 Dopita, M. A., & Evans, I. N. 1986, *ApJ*, 307, 431  
 Drissen, L., & Roy, J.-R. 1994, *PASP*, 106, 974  
 Drissen, L., Roy, J.-R., & Moffat, A. F. J. 1993, *AJ*, 106, 1460  
 Dufour, R. J. 1975, *ApJ*, 195, 315  
 Edmunds, M. G., & Pagel, B. E. J. 1984, *MNRAS*, 211, 507  
 Elmegreen, B. G. 1994, *ApJ*, 427, 384  
 Garnett, D. R. 1990, *ApJ*, 363, 142  
 Gies, D. R., & Bolton, C. T. 1986, *ApJS*, 61, 419  
 Heckman, T. M., Dahlem, M., Lehnert, M. D., Fabbiano, G., Gilmore, D., & Waller, W. H. 1995, *ApJ*, 448, 98  
 Ho, L. C., & Filippenko, A. V. 1996, *ApJ*, 466, L83  
 Hunter, D. A., & Gallagher, J. S. 1996, *ApJ*, 475, 65  
 Hunter, D. A., Gallagher, J. S., & Rautenkranz, D. 1982, *ApJS*, 49, 53  
 Israel, F. P. 1988, *A&A*, 194, 24  
 Israel, F. P., & de Bruyn, A. G. 1988, *A&A*, 198, 109  
 Israel, F. P., & van Driel, W. 1990, *A&A*, 236, 323  
 Izotov, Y. I., Dyak, A. B., Chaffee, F. H., Foltz, C. B., Kniazev, A. Y., & Lipovetsky, V. A. 1996, *ApJ*, 458, 524  
 Kinney, A. L. 1994, *ApJ*, 429, 172  
 Kobulnicky, H. A., & Skillman, E. D. 1996, *ApJ*, 471, 211  
 Kobulnicky, H. A., Skillman, E. D., Roy, J.-R., Walsh, J. R., & Rosa, M. 1997, *ApJ*, 477, 679  
 Koo, B.-C., & McKee, C. F. 1992, *ApJ*, 388, 93  
 Leitherer, C. 1990, *ApJS*, 73, 1  
 Leitherer, C., & Heckman, T. M. 1995, *ApJS*, 96, 9  
 Lequeux, J., Maucherat-Joubert, M., Deharveng, J. M., & Kunth, D. 1981, *A&A*, 103, 305  
 Mac Low, M., & McCray, R. 1988, *ApJ*, 324, 776  
 Marlowe, A. T., Heckman, T. M., & Wyse, R. F. G. 1995, *ApJ*, 438, 563  
 Massey, P., Lang, C. C., DeGioia-Eastwood, K., & Garmany, C. D. 1995, *ApJ*, 438, 188  
 Mendoza, C. 1983, in *IAU Symp. 103, Planetary Nebulae*, ed. D. R. Flower (Dordrecht: Reidel), 143  
 O'Connell, J. S., Gallagher, J. S., III, & Hunter, D. A. 1994, *ApJ*, 433, 65  
 Patel, K., & Wilson, C. D. 1995, *ApJ*, 451, 607  
 Prada, F., Greve, A., & McKeith, C. D. 1994, *A&A*, 288, 396  
 Rola, C., & Pelat, D. 1994, *A&A*, 287, 676  
 Roy, J.-R., Aubé, M., McCall, M. L., & Dufour, R. J. 1992, *ApJ*, 386, 498  
 Roy, J.-R., Belley, J., Dutil, Y., & Martin, P. 1996, *ApJ*, 460, 284  
 Roy, J.-R., & Kunth, D. 1995, *A&A*, 294, 432  
 Schild, R. E. 1977, *AJ*, 82, 337  
 Smith, L. F. 1991, in *Wolf-Rayet Stars and Interrelations with Other Massive Stars in Galaxies*, ed. K. A. van der Hucht & B. Hidayat (Dordrecht: Reidel), 601  
 Stone, R. C. 1979, *ApJ*, 232, 520  
 Tenorio-Tagle, G. 1996, *AJ*, 111, 1641  
 Tomita, O., Ohta, K., & Saito, M. 1994, *PASJ*, 46, 335  
 van Rensbergen, W., Vangeverden, D., & de Loore, C. 1996, *A&A*, 305, 825  
 Waller, W. H. 1991, *ApJ*, 370, 144

*Note added in proof.*—We wish to draw attention to the recent discovery of Wolf-Rayet stars in super star cluster A of NGC 1569 by Rosa M. Gonzalez Delgado, Claus Leitherer, Timothy Heckman, & Miguel Cerviño (*ApJ*, in press [1997]).